

## CHARGED PARTICLE DETECTION AT ELI-NP

O. TESILEANU<sup>1\*</sup>, M. GAI<sup>2,3</sup>, A. ANZALONE<sup>4</sup>, C. BALAN<sup>1</sup>, J.S. BIHALOWICZ<sup>5</sup>, M. CWIOK<sup>5</sup>,  
W. DOMINIK<sup>5</sup>, S. GALES<sup>1</sup>, D.G. GHIȚĂ<sup>1,6</sup>, Z. JANAS<sup>5</sup>, D.P. KENDELLEN<sup>7,3</sup>, M. LA  
COGNATA<sup>4</sup>, C. MATEI<sup>1</sup>, K. MIKSZUTA<sup>5</sup>, C. PETCU<sup>1</sup>, M. PFÜTZNER<sup>5</sup>, T. MATULEWICZ<sup>5</sup>,  
C. MAZZOCCHI<sup>5</sup>, C. SPITALERI<sup>4</sup>

<sup>1</sup>ELI-NP, "Horia Hulubei" National Institute for Physics and Nuclear Engineering, 30  
Reactorului Street, RO-077125, Bucharest-Magurele, Romania

<sup>2</sup>Laboratory for Nuclear Science at Avery Point, University of Connecticut, 1084 Shennecossett Rd.,  
Groton, CT 06340-6097, USA

<sup>3</sup>Department of Physics, Yale University, 217 Prospect Street, New Haven, CT 06511-8499, USA

<sup>4</sup>Istituto Nazionale di Fisica Nucleare, Laboratori Nazionali del Sud, Via Santa Sofia 62, 95123  
Catania, Italy

<sup>5</sup>Faculty of Physics, University of Warsaw, ul. Pasteura 5, 02-093 Warsaw, Poland

<sup>6</sup>"Horia Hulubei" National Institute for Physics and Nuclear Engineering, 30  
Reactorului Street, RO-077125, Bucharest-Magurele, Romania

<sup>7</sup>Triangle Universities Nuclear Laboratory, P.O. Box 90308, Durham, NC 27708-0308, USA

\*Corresponding author *E-mail*: ovidiu.tesileanu@eli-np.ro

*Abstract.* We propose charge particle detectors to be used in measurements utilizing intense gamma-ray beams from the newly constructed ELI-NP facility at Magurele, Bucharest in Romania. We consider a large area Silicon Strip Detector (SSD) and a gas Time Projection Chamber detector read by an electronic readout system (e-TPC). We intend to use the SSD and e-TPC detectors to address essential problems in nuclear structure physics, such as clustering and the many alpha-decay of light nuclei such as  $^{12}\text{C}$  and  $^{16}\text{O}$ . The e-TPC detector may be also used for studies in nanodosimetry and radiation damage to DNA (research described in the Medical Applications TDR of ELI-NP, RA4-TDR5). Both detectors (SSD and e-TPC) will be used to address central problems in nuclear astrophysics such as the astrophysical cross section factor of the  $^{12}\text{C}(\alpha,\gamma)$  reaction and other processes central to stellar evolution. We identify the infrastructure required in Romania and other countries to facilitate the construction of these detectors as well as the required budget and personnel. Memorandums of Understanding (MOUs) between the ELI-NP facility and the collaborating institutes have been signed in order to permit the realization of this Technical Design Report (TDR).

*Key words:* silicon-strip detectors, TPC, charged particle, photon-induced, gamma beam.

## 1. INTRODUCTION AND PHYSICS CASES

The detection of charged particles is a key topic for a Nuclear Physics facility, being important for a wide range of experiments. At Extreme Light Infrastructure – Nuclear Physics (ELI-NP), in order to take advantage of the unprecedented characteristics of its monochromatic gamma radiation beam, state of the art detectors are envisaged. The ELI-NP Technical Design Report (TDR) devoted to the detection of charged particles proposes the construction of two detection systems, described in the following, with their scientific scope that was also described in the ELI-NP review paper [1].

### 1.1 Nuclear Structure

The recent developments in ab-initio calculations of light nuclei (and especially  $^{12}\text{C}$ ) gave fresh momentum to the study of the structure of light nuclei and clustering. The clustering phenomena occurring in cluster models [2, 3] get a microscopic foundation from the theoretical ab-initio shell model [4] and symmetry inspired shell model [5] calculations, ab-initio Effective Field Theory (EFT) calculations on the lattice [6, 7], Fermionic Molecular Dynamics (FMD) model [8] and Antisymmetrized Molecular Dynamics (AMD) model [9]. The structure of the three alpha-particles in the Hoyle state at 7.65 MeV in  $^{12}\text{C}$  and the Hoyle rotational band built on top of the Hoyle state [10, 11, 12, 13, 14] are topics of high interest [15].

The identification of the  $2^+$  member of the Hoyle rotational band was recently proven in an experiment performed at HIγS gamma-ray facility [16] with the optical-readout TPC (O-TPC) [17]. Among the Nuclear Structure studies proposed to be performed at ELI-NP with the e-TPC and SSD detectors are the measurements of the multi-alpha decay of  $^{12}\text{C}$  and  $^{16}\text{O}$ . Similar measurements in other light nuclei will lead to a new perspective on the clustering phenomena these nuclei. Previous studies on the multi-alpha decay of  $^{12}\text{C}$  were performed with Silicon Strip Detectors (SSD) [18, 19, 20].

A detailed description of this physics topic at ELI-NP is given in [1].

### 1.2 Nuclear Astrophysics

With the proposed detectors and using the gamma radiation beam with unique characteristics at ELI-NP, we will be able to respond to the need of Nuclear Astrophysics to perform accurate measurements of (very small) cross sections of nuclear reactions of the hydrogen and helium burning processes and hence the astrophysical S-factor (as defined in [21]) that are essential for stellar evolution

theory. Measuring capture reactions by means of the inverse photodisintegration reaction, besides being inherently low background measurements, have the advantage of having a different systematic uncertainty than those of characteristic charged particle induced reactions measured at low energies of astrophysical interest. Such systematic issues for example involving the target and its deterioration, (effective) beam energy definition, etc., lead to different systematic errors and thus may allow us to resolve conflicting data.

We refer the reader to [21] for a thorough review of stellar evolution theory and the definition of the nomenclatures used in this field and this paper.

Part of the proposed studies in this field using the charged particle detectors at ELI-NP were presented in [1], namely the  $^{16}\text{O}(\gamma,\alpha)^{12}\text{C}$ ,  $^{24}\text{Mg}(\gamma,\alpha)^{20}\text{Ne}$  and p-process reactions. Some of the other reactions proposed are reviewed in the following sections.

### 1.2.1 The $^{22}\text{Ne}(\gamma,\alpha)^{18}\text{O}$ Reaction

One of the neutron sources for *s*-process nucleosynthesis in massive stars is the  $^{22}\text{Ne}(\alpha,n)^{25}\text{Mg}$  reaction. This reaction plays a non-negligible role also at lower temperatures in low-mass stars, where the main neutron source is the  $^{13}\text{C}(\alpha,n)^{16}\text{O}$  reaction. The observed abundance patterns are strongly influenced by the  $^{22}\text{Ne}(\alpha,n)^{25}\text{Mg}$  reaction. Clarifying the way in which these two reactions compete, is still an open challenge. This challenge stems from the uncertainties for the reaction rates at the relevant temperatures in either astrophysical site.

The seed nucleus  $^{22}\text{Ne}$  is produced after the CNO-driven burning phase of massive stars, through the helium-burning of oxygen,  $^{18}\text{O}(\alpha,\gamma)^{22}\text{Ne}$ . The experimental knowledge of the latter reaction underwent considerable progress over recent years, with the study of the low-lying resonances at 566 and 470 keV [22]. This study yielded resonance strengths of  $0.71 \pm 0.17 \mu\text{eV}$  and  $0.48 \pm 0.16 \mu\text{eV}$ , respectively. Still, in particular for the lower-energy resonance, uncertainties need to be reduced. Such resonance strengths are at the limits of the experimental capabilities for study in direct reactions, but are rather strong for measuring in the inverse photodisintegration reactions.

#### **Design Goal (e-TPC):**

The proposed measurements of these two low-energy resonances have the following characteristics (with an e-TPC operating at 100 mbar with  $^{22}\text{Ne}$  gas as discussed in Section 3 of the TDR):

*566 keV resonance:*  $\gamma$ -ray beam energy 10.13 MeV,  $^{18}\text{O}$ -recoil energy 121 keV,  $\alpha$ -particle energy 445 keV,  $^{18}\text{O}$  recoil range 10(3) mm and  $\alpha$ -particle range 80(7) mm;

*470 keV resonance:*  $\gamma$ -ray beam energy 10.05 MeV,  $^{18}\text{O}$ -recoil energy 85 keV,  $\alpha$ -particle energy 385 keV,  $^{18}\text{O}$  recoil range 7(2) mm and  $\alpha$ -particle range 62(6) mm.

Assuming a conservative beam intensity of  $2.5 \times 10^4$   $\gamma$ /s/eV, beam width of 0.5%, target thickness  $8.5 \times 10^{19}$  atoms/cm<sup>2</sup> (100 mbar <sup>22</sup>Ne), we expect count rates of 7 and 1 event/hour for the 566 and 470 keV resonances, respectively.

### 1.2.2 The <sup>19</sup>F( $\gamma$ ,p)<sup>18</sup>O Reaction

In population I (high-metallicity) stars with masses larger than the mass of the Sun, the CNO cycles are responsible for most of the hydrogen burning [23]. Hydrogen burning of <sup>18</sup>O, resulting from the  $\beta$ -decay of <sup>18</sup>F, can occur through two competing reactions: <sup>18</sup>O(p, $\gamma$ )<sup>19</sup>F and <sup>18</sup>O(p, $\alpha$ )<sup>15</sup>N. Of these, the latter leads to a recycling of the CNO catalytic material into the CN cycle [24] and dominates the hydrogen burning. On the other hand, the former may generate a small leakage from the CNO cycle to the subsequent burning of <sup>19</sup>F through <sup>19</sup>F(p, $\gamma$ )<sup>20</sup>Ne. The <sup>18</sup>O(p, $\gamma$ )<sup>19</sup>F reaction could be the origin of the loss of catalytic materials from the CNO cycle, providing at the same time a link to the NeNa cycle. An understanding of this reaction at the relevant energies ( $T \leq 1$  GK) is crucial in order to determine the amount of catalytic material lost by the cycle. It is also needed in order to locate the Ne-Na nucleosynthesis site.

At relatively low temperatures ( $T \leq 1$  GK), the <sup>18</sup>O(p, $\gamma$ )<sup>19</sup>F reaction ( $Q = 7.994$  MeV) is dominated by several resonances. The resonance strength of most resonances at excitation energies corresponding to  $T \geq 0.1$  GK has already been measured [25, 26, 27]. At lower temperatures,  $T \leq 0.1$  GK, large uncertainties dominate the experimental information available. In particular, the resonance at  $E_{c.m.} = 90$  keV has not been observed in the (p, $\gamma$ ) channel, yet. Only an upper limit of  $\omega\gamma \leq 7.8 \times 10^{-9}$  eV could be recently inferred [27].

#### Design Goal (e-TPC):

This low-energy resonance has the following characteristics (with e-TPC operating at 100 mbar CF<sub>4</sub> gas as discussed in Section 3):  $\gamma$ -beam energy 8 MeV, <sup>18</sup>O-recoil energy 5 keV,  $\alpha$ -particle energy 85 keV, <sup>18</sup>O recoil range less than 200  $\mu$ m and proton range 7(1) mm. Assuming a conservative beam intensity of  $2.5 \times 10^4$   $\gamma$ /s/eV, beam width of 0.5%, target thickness  $3.40 \times 10^{20}$  atoms/cm<sup>2</sup> (100 mbar CF<sub>4</sub>), we expect a count rate of 5 events per day for the very low energy resonance at  $E_{c.m.} = 90$  keV.

### 1.2.3 The <sup>21</sup>Ne( $\gamma$ , $\alpha$ )<sup>17</sup>O Reaction

The first direct measurement of the <sup>17</sup>O( $\alpha$ , $\gamma$ )<sup>21</sup>Ne reaction [28] revealed resonances at  $E^* = 8.159(2)$ ,  $8.470(2)$  and  $8.659(2)$  MeV in <sup>21</sup>Ne. The determination

of the cross section of the  $^{17}\text{O}(\alpha,\gamma)^{21}\text{Ne}$  reaction at lower energies is essential for determining the role of  $^{16}\text{O}$  as a neutron poison since it can readily capture neutrons to form  $^{17}\text{O}$ . The strength of the  $^{17}\text{O}(\alpha,\gamma)^{21}\text{Ne}$  reaction as compared to the  $^{17}\text{O}(\alpha,n)^{20}\text{Ne}$  reaction, determines the efficiency of the  $^{16}\text{O}$  for neutron poisoning. As discussed in [28] “due to the occurrence of resonances in  $^{18}\text{O}(\alpha,n_1)^{21}\text{Ne}$  as well as in the  $^{17}\text{O}(\alpha,n_1)^{20}\text{Ne}$  reaction [their] observed  $\gamma$  -spectrum contained many strong background and neutron induced lines complicating the identification of resonant  $\gamma$ -ray transitions”. In addition spin-parity assignments could not be established for the two higher energy resonances (the 8.159 MeV state was already known to have the  $J^\pi = 9/2^+$ ). The use of gamma-beams at the ELI-NP facility will remove such background(s) and will allow for measurements of the spin parity as well as new measurements of states at lower energies (e.g.  $E^* = 8.065, 8.008$  MeV etc.) which are very important for evaluating the cross sections at stellar conditions.

**Design Goal (e-TPC):**

The measured resonance strength [28] of more than 1 meV will allow us to re-measure these resonances using e-TPC operating at 100 mbar with  $^{21}\text{Ne}$  isotopic gas in measurements lasting only a few hours, since rates of a few tens of events/hour are expected under conservative conditions (assuming a conservative beam intensity of  $2.5 \times 10^4$   $\gamma$ /s/eV, beam width of 0.5%). New measurements of the lower energy resonances at, e.g. 8.065 and 8.008 MeV) will be possible provided the resonance strength is larger than 1  $\mu\text{eV}$ . For such values rates of few events/day can be expected.

## 2. TECHNICAL PROPOSAL

### 2.1 The Large Area Silicon Strip Detector

The reactions presented in Section 2, all have charged particles in the exit channel. Silicon detectors represent one of the best solution for their detection for a number of reasons: (i) they guarantee exceptional energy resolution, (ii) they have almost 100% efficiency in charged particle detection, (iii) thresholds can be set to very small values, (iv) they are not sensitive or very little sensitive to neutrons, gamma rays and electrons, which would constitute the beam induced background.

Moreover, silicon detectors will allow for particle identification through time-of-flight measurement and pulse shape analysis, by exploiting the time structure of the photon beam and by implementing a fast ADC readout of the strip detectors. Alternatively, particle identification (ID) could be achieved by introducing thin silicon detectors to measure the energy loss and perform particle identification through the  $\Delta E$ -E technique.

A silicon array would make it possible to measure reactions on solid targets, such as the  $^{24}\text{Mg}(\gamma,\alpha)^{20}\text{Ne}$  and all the reactions on heavy nuclei intervening in the p-process ( $^{74}\text{Se}$ ,  $^{78}\text{Kr}$ ,  $^{84}\text{Sr}$ ,  $^{92}\text{Mo}$ , and  $^{96}\text{Ru}$ , for instance), brought as an example in the previous section, representing a complementary detector to the TPC detector we discuss below in Section 3.2. In the case of other reactions that could be induced on gas species, measurements with the silicon array would be useful to reduce systematic uncertainties, since various sources of systematic errors contribute in the two cases.

Excitation functions and angular distributions can be measured over a wide range allowing for a better understating of reaction mechanism. Taking into account the presence of beam induced background at forward angles, an angular coverage as large as  $10^\circ$ - $170^\circ$  can be achieved in the lab system, which is a range large enough to perform an effective nuclear spectroscopy. Silicon strip detectors would couple enhanced angular and energy resolution with high detection efficiency. Such resolution can be important for background suppression owing to, for instance, the bremsstrahlung radiation component. High granularity is not a crucial aspect as a low counting rate is expected, making the probability of multiple hits very small.

Since absolute cross sections are to be measured, accurate gamma beam monitoring systems have to be developed, aiming at measuring the photon spectrum with accuracy better than 5% to keep the overall uncertainty affecting the measured cross section at the 10% level.

In the past years, SSD arrays have been successfully designed for application to nuclear astrophysics. In particular, the ORRUBA [29] and ANASEN [30] detectors seem to fit very well with the technical requirements mentioned so far.

These arrays are made up of X3 silicon-strip detectors manufactured by Micron Semiconductor Ltd [31] arranged into a barrel configuration. The X3 are 4-strip detectors 4 cm wide, position sensitive along the longitudinal axis (7.5 cm long) thanks to the charge division technique, leading to a position resolution better than 1 mm (FWHM). The position resolution was measured, for instance, by [29] (see Fig. 1). The barrel can be made up of 3 rings of 12 position sensitive detectors, for a total angular coverage of  $100^\circ$  in the laboratory system. This setup results in a very compact design as the distance target - detector is about 9 cm, fixing  $\Delta\phi = 6.5^\circ$  and  $\Delta\theta = 0.6^\circ$ , which is a satisfactory angular resolution for reaction such as  $^{24}\text{Mg}(\gamma,\alpha)^{20}\text{Ne}$ . Energy resolution better than 1% is measured with a calibration alpha source [30]. Since position is determined by charge partition, the number of electronic channels is strongly reduced, as about 300 channels would be necessary for the whole barrel.

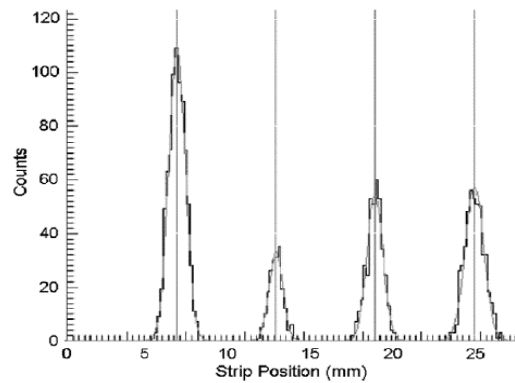


Fig. 1 - Plot of strip position for collimated protons elastically scattered from a gold target at 11.5 MeV. The slot widths corresponding to the peaks were, from left to right, 1.0, 0.5, 1.0 and 1.5 mm. The fit to the peak corresponding to the 0.5 mm slot yielded a position resolution of 0.5 mm (FWHM) [29].

The angular coverage is extended down to about  $20^\circ$  ( $160^\circ$  at backward angles) by using end cap detectors such as the assembly of four QQQ3 segmented detectors by Micron Semiconductor Ltd [31]. Each quadrant of the QQQ3 is segmented into 16 radial segments (3 mm pitch) and 16 angular segments [30], with inner and outer radii of 5 and 10 cm, respectively. If necessary, smaller angles can be covered by adding additional smaller rings at the two ends of the barrel.

The scattering chamber housing this detector array must have a diameter of at least 40 cm, while the space required for the full setup (including electronics) is about 1.5 m. Standard vacuum has to be provided inside the scattering chamber. It should also accommodate a remotely controlled target ladder and the detector mounting has to foresee a position calibration system, made up of a mask with equally spaced holes of known position.

Because of the compact design of the detector, time-of-flight cannot be used for particle ID. However, pulse shape analysis (PSA) has proved effective down to about 2 MeV, still making it possible to identify the impinging nuclei [32]. This has been achieved with neutron transmutation doped (NTD) silicon detectors, guaranteeing high electric field uniformity within their volume. The use of position sensitive detectors might allow one to use PSA even for less uniform detectors; tests are presently ongoing.

Since other silicon strip detector assemblies to detect charged particles from photo-dissociation events at ELI-NP are possible (for instance, a silicon ball or a barrel of double sided silicon strip detectors), we have performed GEANT4 simulations of the experimental setup to optimize resolution, detection efficiency, compactness, granularity, possibility of particle identification and costs. According

to our simulations, the barrel configuration (Fig. 2) represents the best configuration, both on the technical point of view and for its cost.

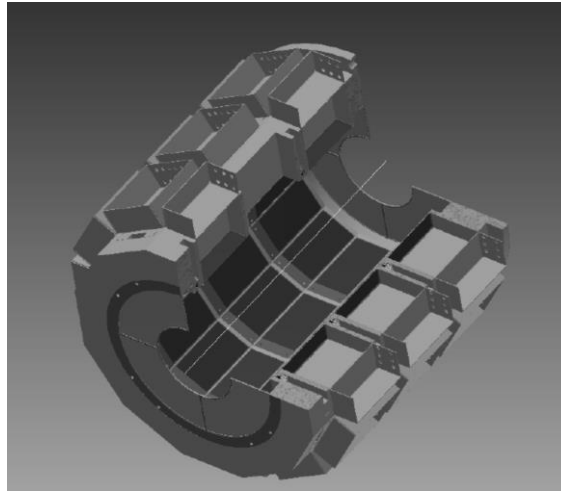


Fig. 2 - Drawing of the proposed silicon array.

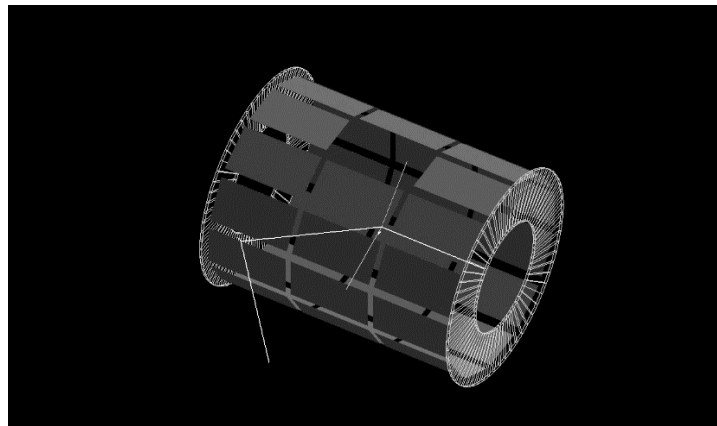


Fig. 3 - Simulated charged particle detector made up of X3 silicon-strip detectors (green pads) arranged into a barrel configuration and QQQ3 endcap detectors (yellow strips). A photo-dissociation event is shown, where an impinging photon (right to left) hits a  $^{24}\text{Mg}$  target producing an outgoing alpha particle (yellow track), a recoil  $^{20}\text{Ne}$  nucleus (red track) and a photon from  $^{20}\text{Ne}$  de-excitation (white track). The emitted gamma-ray later undergoes Compton scattering from the scattering chamber (not shown).

In Fig. 3 a simulated photo-dissociation event is displayed, in the case of a gamma ray hitting a  $^{24}\text{Mg}$  target. To show the detector, green pads are used for the X3 silicon-strip detectors and yellow strips for QQQ3 endcap detectors. Since X3 detectors are made up of four strips, each position sensitive and 10 mm wide, the chances of multiple hits are very small (less than 0.1% in the worst case, namely, reactions with at least 3 particles in the exit channel). This means that granularity is good enough to guarantee a negligible systematic error. At the same time, resolution on the zenith angle is better than 0.5 degrees (on the azimuth angle is ten times larger, but this angle is not critical for astrophysical measurements), well suited for astrophysical reactions. This good angular resolution is very important to allow the kinematical identification of reactions.

A compact device such as the barrel detector array would make it impossible to use ToF for particle identification. Owing to the low particle energies, since nuclear astrophysics reactions are induced at photon energies slightly larger than particle emission thresholds, the standard is induced at photon energies slightly larger than particle emission threshold introduced. In the same way, pulse shape analysis has presently proven impossible at such low energies, making kinematical identification the only viable option to separate the reaction of interest from others at present.

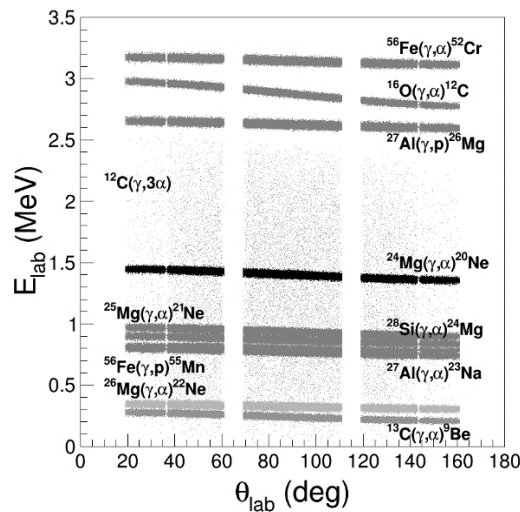


Fig. 4 - Summary of the kinematics of the reactions induced by 11 MeV gamma ray on  $^{24}\text{Mg}$  and on a variety of contaminants possibly present in the target or in the backing, and in the detectors and target holders. Energy resolution is taken into account.

Using a Monte Carlo simulation we have investigated the possibility to use kinematics to disentangle the channel of interest from background processes. We have evaluated the particle yield from gamma interaction with a  $^{24}\text{Mg}$  target and other nuclei that may be present in the chamber, as contaminants or in the gamma ray path. Fig. 4 shows the energies and angles of emission of the light fragment for the indicated reactions. With the exception of the  $^{12}\text{C}(\gamma,3\alpha)$  reactions, the kinematic loci are well separated from the one of the  $^{24}\text{Mg}(\gamma,\alpha)^{20}\text{Ne}$  reaction. Energy resolution is accounted for as given in the ELI-NP specification (FWHM = 35 keV at 11 MeV beam energy). However, since the  $^{12}\text{C}(\gamma,3\alpha)$  reaction has three particles in the exit channels, a very different kinematics is expected, making it straightforward to disentangle the contribution of the  $^{24}\text{Mg}(\gamma,\alpha)^{20}\text{Ne}$  reaction from the one from the  $^{12}\text{C}(\gamma,3\alpha)$  process.

This is clearly seen in Fig. 5. It is worth noting that the relative height of each peak has no physical meaning, as it is linked to phase space population only (no reaction dynamics included so far). A broad distribution is found for the  $^{12}\text{C}(\gamma,3\alpha)$  reaction (given in dark blue), covering the 0 – 2.5 MeV energy region, since three particles are present in the exit channel. Within the energy range spanned by the  $^{24}\text{Mg}(\gamma,\alpha)^{20}\text{Ne}$  reaction, the contribution of the  $^{12}\text{C}(\gamma,3\alpha)$  is even negligible, unless reaction dynamics changes the cross section ratio by orders of magnitude.

From the previous spectra, it turns out that kinematic identification of the  $^{24}\text{Mg}(\gamma,\alpha)^{20}\text{Ne}$  reaction is very effective and background should be negligible. Similar considerations applies to other reactions we have included in our proposal, namely, the  $^{96}\text{Ru}(\gamma,\alpha)^{92}\text{Mo}$  and  $^{74}\text{Se}(\gamma,p)^{73}\text{As}$ . These give ejectiles of energies larger than 3.5 MeV, so the contribution of contaminants is absent.

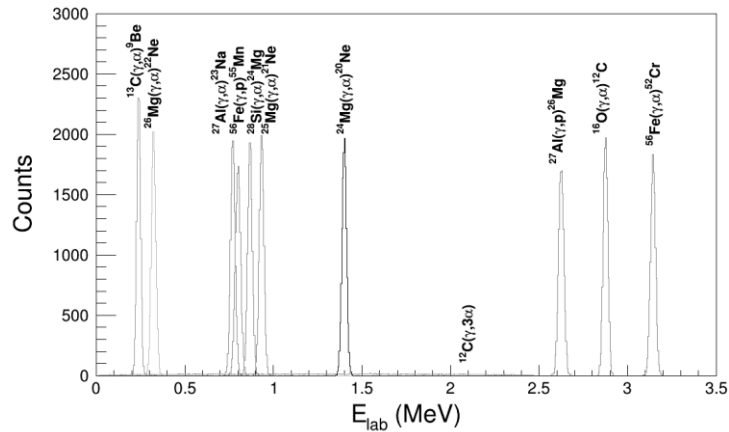


Fig. 5 - Energy spectrum as detected into a X3 detector at a fixed angle of  $90 \pm 5$  degrees. The  $^{12}\text{C}(\gamma,3\alpha)$  locus (given in dark blue) covers the 0 – 2.5 MeV energy region. A broad distribution is found as three particles are present in the exit channel.

Besides direct gamma beam (at a fixed energy, if energy spread is neglected) particles may hit the detectors following the interaction of a Compton scattered photon with detector holders, the scattering chamber and detector themselves. Therefore, we have determined the spectrum of backscattered gamma rays in the worst case, that is, the absence of any beam stop. From Fig. 6 it is apparent that the fraction of backscattered photons whose energies exceed a typical particle emission threshold (4 MeV) is negligible.

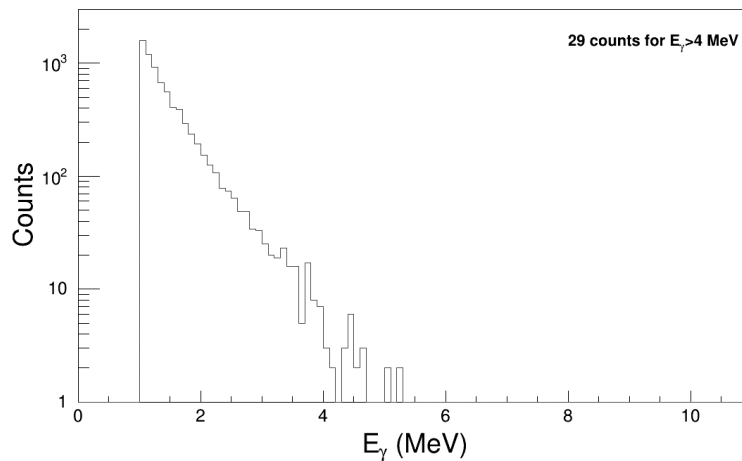


Fig. 6 - Spectrum of backscattered gamma rays under the hypothesis no beam stop is present. The amount of photons possibly causing particle emission is negligible. In the Monte Carlo calculation,  $10^7$  impinging photons were considered.

Regarding the ancillary electronics, the readout of the silicon strip detectors will be performed by using the GET electronics, discussed in details in Section 2.2. This would ensure high resolution keeping costs low and strongly reducing the bulk of the front-end electronics, as one board can process 256 signals. Taking into account that the use to charge-partition silicon strip detectors allows us to 311 channels, it means that two boards would be necessary to handle the whole detector readout. Research and development activity would be necessary to adapt the GET electronics, introduced for TPC detectors, to silicon strip detectors. For instance, suited preamplifiers have to be implemented to guarantee the best energy and position resolution and proper coupling with the GET readout. An additional advantage of the adoption of the GET system is the possibility to have common electronics and DAQ systems with other experiments to be installed at the ELI-NP facility, leading to a standardization of the readout systems strongly enhancing the efficiency of the setups.

### 2.1.1 Why two Silicon-Strip Detector arrays at ELI-NP

Two detector arrays based on SSDs are proposed in the TDRs for experiments at ELI-NP. This section explains the differences between them, demonstrating there's no duplication in the applicability.

In photo-disintegration reactions of astrophysical relevance (studies proposed in this TDR), particles can be emitted with energies as low as few hundreds keV, owing to the comparatively low photon energies in stars, of the order of about 10 MeV during the latest stages of stellar evolution (pre supernova conditions). Such energies are slightly larger than particle emission thresholds, thus a close link with nuclear structure considerations and nuclear spectroscopy is apparent. Under these conditions, no  $\Delta E$  detectors can be used for particle ID unless an untenable detection threshold is introduced, strongly limiting our access to the relevant energy interval. Pulse Shape Analysis (PSA) has proved not applicable yet at such energies while time-of-flight measurement would imply a very large detector, entailing very high costs to guarantee the necessary high energy and angular resolution, which are especially important for nuclear spectroscopy. Therefore, we plan to perform particle ID by means of full reconstruction of reaction kinematics. Thanks to the high energy and angular resolution (about 0.5% and 0.2 degrees, respectively) and the broad angular coverage, the kinematics of the different reactions can be disentangled and, consequently, the signal can be separated from background processes, if present. Since few particles are emitted per reaction event, low granularity is sufficient, allowing us to keep the number of electronic channels comparatively low by using charge partition position sensitive detectors. It is important to underline that no digitalization of the signal is necessary, since PSA is not viable, so a small data flow will be produced as few detectors will be fired. On the other hand, the request of high resolution implies the usage of suitable electronics; for instance, standard analog electronics would perfectly match the required resolution standards still being a viable solution thanks to the total number of channels necessary (about 400). Regarding radioprotection issues, no significant radioactivity is produced since ( $\gamma, \alpha$ ) and ( $\gamma, p$ ) reactions are mostly studied. This allows us to operate on the chamber to replace targets and study different photo-dissociation reactions in the measurement campaign.

In the case of photo-fission reactions (the other ELI-NP TDR employing SSDs), the physical conditions are quite different, requiring a different approach. First of all, photo-fission processes involve the emission of a large number of energetic fragments. This implies the necessity of accurate particle identification and a large granularity to prevent multiple hits. This can be achieved by using double-sided silicon strip detectors coupled with PSA. No kinematic identification would be possible as a large number of fragments is emitted and because of the different physics leading to the fragment production (such as secondary emission of fragment

and in-flight decay). The large number of electronic channels requested by double-sided silicon strip detectors makes it necessary the use of ASIC electronics, while the digitalization of signals from each strip would produce a large data output, calling for a devoted high speed acquisition system. Double-sided silicon strip detectors would guarantee the needed energy and angular resolution. Regarding radioprotection issues, the study of photo-fission on actinide (usually radioactive) targets cannot avoid contaminating the detectors with fission fragments and maybe even with long lifetime actinides. Therefore a dedicated detector set-up is necessary, besides the previous consideration based on the different physics to be investigated, which will be used only for this purpose. For radiation safety reasons a dedicated laboratory would be necessary to manipulate the detectors and the other irradiated material

### 2.1.2 Comparison with existing apparatus

The SSD array to be installed at ELI-NP has been devised with the aim to provide an almost  $4\pi$  solid angle coverage coupled with high energy and angular resolution and low thresholds. These requests are closely linked to the distinct features of photo-dissociations reactions, for nuclear structure and, in particular, for nuclear astrophysics. Indeed, clustering phenomena and nuclear processes of astrophysical impact occur at photon energies close to the particle emission threshold, making it necessary to detect low energy light ions (namely, protons and  $\alpha$  particles of energies as low as few hundreds keV). Therefore, no particle ID through standard energy loss vs. residual energy study is viable, neither time-of-flight measurements unless large detectors are implemented. In the same way, standard pulse-shape analysis is not able to disentangle detected particle A and Z at such low energies.

For these reasons our detector perfectly matches the physics to be investigated at the ELI-NP facility, with respect to both the choice of detectors and geometry and of the ancillary electronics. Low-threshold,  $4\pi$  coverage and high energy and angular resolution allows for a high efficiency background rejection through kinematical particle ID, a full event reconstruction for very accurate nuclear spectroscopy and an almost 100% detection efficiency, allowing us to cover unexplored energy regions of paramount nuclear astrophysics and nuclear structure relevance, only possible with ELI-NP high intensity and resolution  $\gamma$  beam. Regarding the electronics, a significant contribution to the performances and the flexibility of the system is given by the adoption of the GET electronics, modified to match silicon detectors.

Existing  $4\pi$  detectors, such as the ORRUBA or the ANASEN arrays, though using similar array shapes (barrel assembly) and detectors (the X3 and the QQQ3 detectors manufactured by Micron Semiconductors) were devised for different studies, namely the investigation of nuclear reactions induced by charged particles,

at energies well above the particle emission thresholds. The main purpose was the investigation of transfer reactions for spectroscopic purposes, especially induced by radioactive ion beams, or the measurement of excitation functions by means of the thick target approach (by filling the scattering chamber with a suitable gas, in the case of the ANASEN detector). The ANASEN array is much more complicated as it is coupled with a wire chamber for trajectory reconstruction. Moreover, since high-energy particles have to be detected, scintillation detectors are used to fully stop the ejectiles. As such, a primary goal of both detectors was a large solid angle coverage (owing to the low intensity of radioactive ion beams) while resolution had a less important role, being the beam quality of such beams much worse than planned at ELI-NP. In the same way, the problems of detection thresholds and pulse shape analysis were not addressed, which represent a key aspect of the present array.

In conclusion, we can state the availability of extreme quality and intensity  $\gamma$  beam at ELI-NP has triggered a revision of existing silicon arrays to make it possible to investigate previously inaccessible nuclear processes, both regarding energy and resolution, to provide a perfect matching between the beam properties and the detector performances. Such coupling of state of the art  $\gamma$  beam, electronics and silicon detectors will lead to a significant improvement of the physics of photo-dissociation reactions for nuclear astrophysics and nuclear structure studies.

## 2.2 Time Projection Chamber (TPC) Detector

The detector which is most suitable to investigate the multi alpha-particle decay of light nuclei such as  $^{12}\text{C}$  and  $^{16}\text{O}$  and the cross section of astrophysical relevant photo-dissociation reactions  $(\gamma, p)$  or  $(\gamma, \alpha)$  that were discussed above in Section 2, is a gaseous detector (unless a solid target is required) in which the gas acts at the same time as target for the nuclear reaction and detection medium. For this purpose an active target TPC with electronic readout (e-TPC) is proposed.

The active volume of the chamber, in which the reaction happens and the decay products are detected, will have a length of 35 cm and a square cross-section of  $20 \times 20 \text{ cm}^2$ , centered around the beam axis with a window for the gamma beam and another on the side for an alpha source. The schematic diagram of the e-TPC detector is shown in Fig. 7. In Fig. 8 we show a typical  $\alpha + ^{12}\text{C}$  event from the photo-dissociation of  $^{16}\text{O}$  measured at the HI $\gamma$ S facility [17, 16] and in Fig. 9 we show a typical recorded event of two proton decay of  $^{45}\text{Fe}$  measured at the at the National Superconducting Cyclotron Laboratory (NSCL) facility at Michigan State University (MSU) [33].

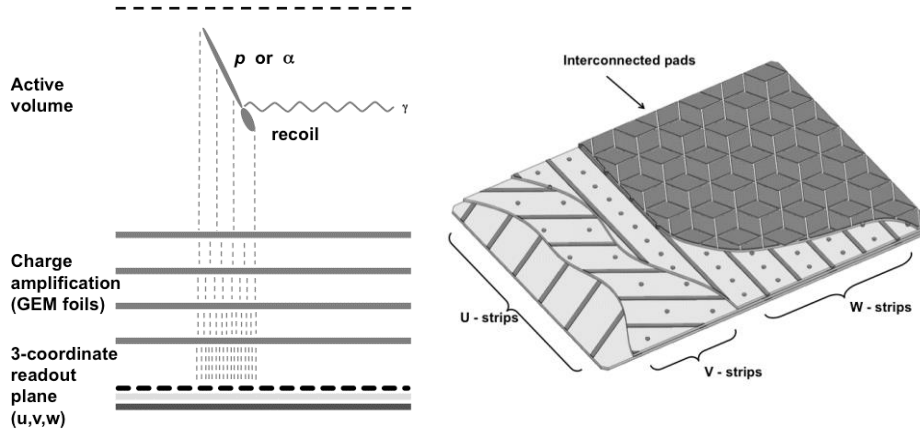


Fig. 7 - Left panel: A schematic diagram of the gaseous e-TPC detector equipped with GEM structure and a planar electronic readout. Right panel: structure of the charge-collecting 3-coordinate (u-v-w) electrode [34].

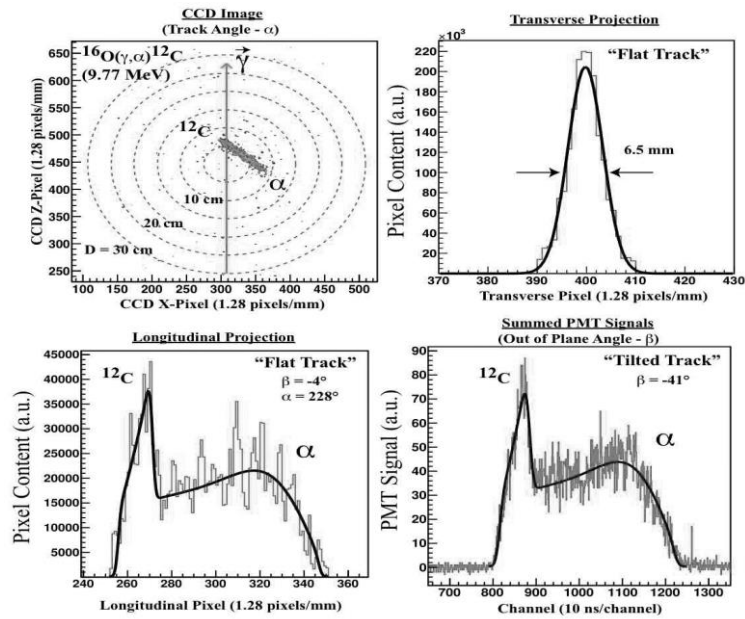


Fig. 8 - A typical  $\alpha + {}^{12}\text{C}$  event recorded by the O-TPC at the HI $\gamma$ S facility as described in details in [17]. © SISSA Medialab Srl. Reproduced by permission of IOP Publishing, all rights reserved.

The multiplication of the drifting electrons will be achieved by a sequence of 35 cm × 20 cm Gas Electron Multiplier (GEM) foils fabricated at CERN. The charge will be read by a u-v-w readout which is mounted on a circuit board using multi-layering board technology, as shown in Fig. 7, and it is formed by three layers of (u-v-w) grids crossed at 60°. The proposed TPC detector is similar to the O-TPC detectors developed and constructed at the University of Warsaw, used to investigate rare decay modes [35, 33, 36, 37, 38] of for example  $^{45}\text{Fe}$  and  $^{48}\text{Ni}$  at the NSCL facility. The University of Connecticut used a low-pressure O-TPC to study the  $^{16}\text{O}(\gamma,\alpha)^{12}\text{C}$  reaction at the HIγS gamma-ray facility [17, 16].

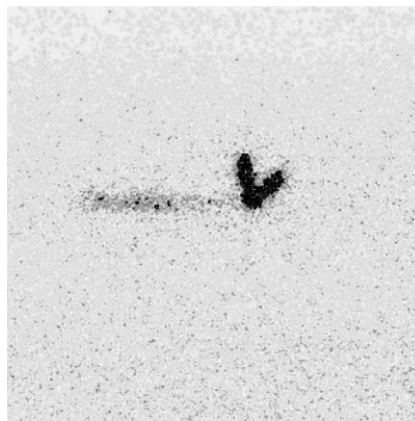


Fig. 9 - A typical two-proton decay event recorded by the O-TPC at the NSCL-MSU facility as described in details in [33].

**The novelty of the proposed e-TPC detector with respect to the previously used O-TPC detectors [35, 17] consists in the proposed readout method, which will provide faster readout and the capability to resolve more complex events topology.** We will replace the optical readout with an electronic readout by means of a charge-collecting electrode plane with the capability of time resolved 2D readout that will be placed at the bottom of the chamber. This flat collecting electrode made out of integrated circuit board is placed behind the last charge-multiplication electrode and it will collect charges from the avalanches. The conducting readout electrode is segmented in strips forming three independent readout lines of the charge position thus forming virtual pixels on the surface organized into the u-v-w geometry, see Fig. 7. These virtual pixels will allow for two-dimensional reconstruction of the reaction products in a given time slice. Synchronous sampling of the pulses collected on the strips will allow to reconstruct the vertical coordinate of each time slice for a given drift velocity.

Combination of the 2D position in the collection plane with time information will allow the 3D reconstruction of the reaction products. This is required in order to extract the reaction angle ( $\theta$ ) and the azimuthal angle ( $\phi$ ). The 3D reconstruction of events will also allow us to identify reactions in which more than two particles are involved, like  $^{12}\text{C}(\gamma,3\alpha)$ , or when more events (including background) happen within a short time-window of the information collection. **For best analysis of the tracks, linearly polarized gammas tilted at  $45^\circ$  with respect to the horizontal plane are assumed.** A strip pitch of 1.5 mm will allow for a space resolution sufficient to identify also short tracks generated by the recoil in the gas (approximately 100 mbar). This read-out mechanism allows reducing the number of readout channels with respect to the classical pixels design for the same area. In Fig. 7 (right panel) a schematic representation of the charge-collecting electrode plane is displayed. The multi-layer printed circuit board of this u-v-w collection plate has been developed for a gas detector to measure X-rays emitted by tokamak plasma [39, 40] and is adopted for the readout of the proposed e-TPC.

The advantages of such a read-out scheme, with respect to the optical readout employed so far are:

1. Compactness of the system: the readout electrode is embedded in the detector body, making the system very compact.
2. High acceptance of the read-out structure to the signals generated.
3. Larger choice of gas mixtures to be used as detection target: only the criterion of stable charge avalanching is applied. The requirement of light emission is no longer needed.
4. Capability of reconstructing more complex reactions (3 or more particles emitted) and of rejecting background events.
5. Possibility to process on-line the signal to be used as first-level event selection.

Moreover, it will have a significantly lower cost with respect to pixel-based read-out due to the smaller number of electronics channels employed.

The detector body will have an entrance window for the beam, as well as an opening to insert an alpha source for calibration and testing purposes. The detector will operate at a gas pressure of the order of 100 mbar, in order to allow for both the recoiling nucleus and the lighter reaction product (proton or alpha) to be stopped and tracked in the chamber's active volume. The reaction products have very different ranges in the gas: they can vary by as much as one order of magnitude for the most asymmetric reactions, see Fig. 10. The two plots displayed in Fig. 10 show the laboratory energy, and consequently range, weak dependence on the angle of the alpha particle in the center of mass, rendering the event reconstruction and identification unambiguous.

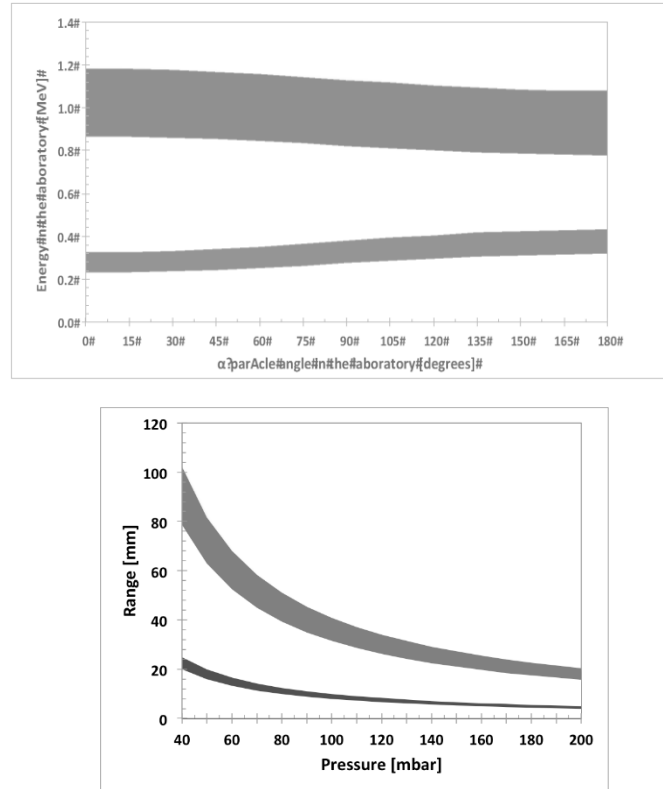


Fig. 10 - Top panel: energy of the particles emitted in the reaction  $^{16}\text{O}(\gamma, \alpha)^{12}\text{C}$  as a function of the alpha-emission angle with respect to the beam direction (all quantities are in the laboratory frame). Energies of  $\alpha$  particles (upper band) and  $^{12}\text{C}$  ions (lower band) are calculated for  $E_\gamma$  between 8.26 MeV and 8.67 MeV ( $E_{c.m.}$  between 1.1 MeV and 1.5 MeV, respectively). Bottom panel: range of the charged particles emitted in reaction  $^{16}\text{O}(\gamma, \alpha)^{12}\text{C}$  as a function of the  $\text{CO}_2$  gas pressure calculated with the SRIM code [41]. The ranges of  $\alpha$  particles and  $^{12}\text{C}$  ions correspond to  $E_\gamma$  between 8.26 and 8.67 MeV and  $90^\circ$  angle with respect to the beam direction.

In order to reduce the background from carbon-induced reactions we proposed to use isotopically enriched  $^{13}\text{CO}_2$  gas with a threshold for particle emission from  $^{13}\text{C}$  of 10.6 MeV. The use of the isotopically enriched  $^{13}\text{CO}_2$  gas is essential for measuring at very low energies ( $E_\gamma \sim 8$  MeV) the cross section of the  $^{16}\text{O}(\gamma, \alpha)^{12}\text{C}$  reaction.

Hence we proposed to construct the gas recycling system shown in Fig. 11. We note that the very same gas system is now being constructed by the UConn-TUNL collaboration at the HI $\gamma$ S facility and experience gained at HI $\gamma$ S facility will again aid our project at the ELI-NP facility. Isotopically enriched gasses will be needed also for several of the other proposed experiments.

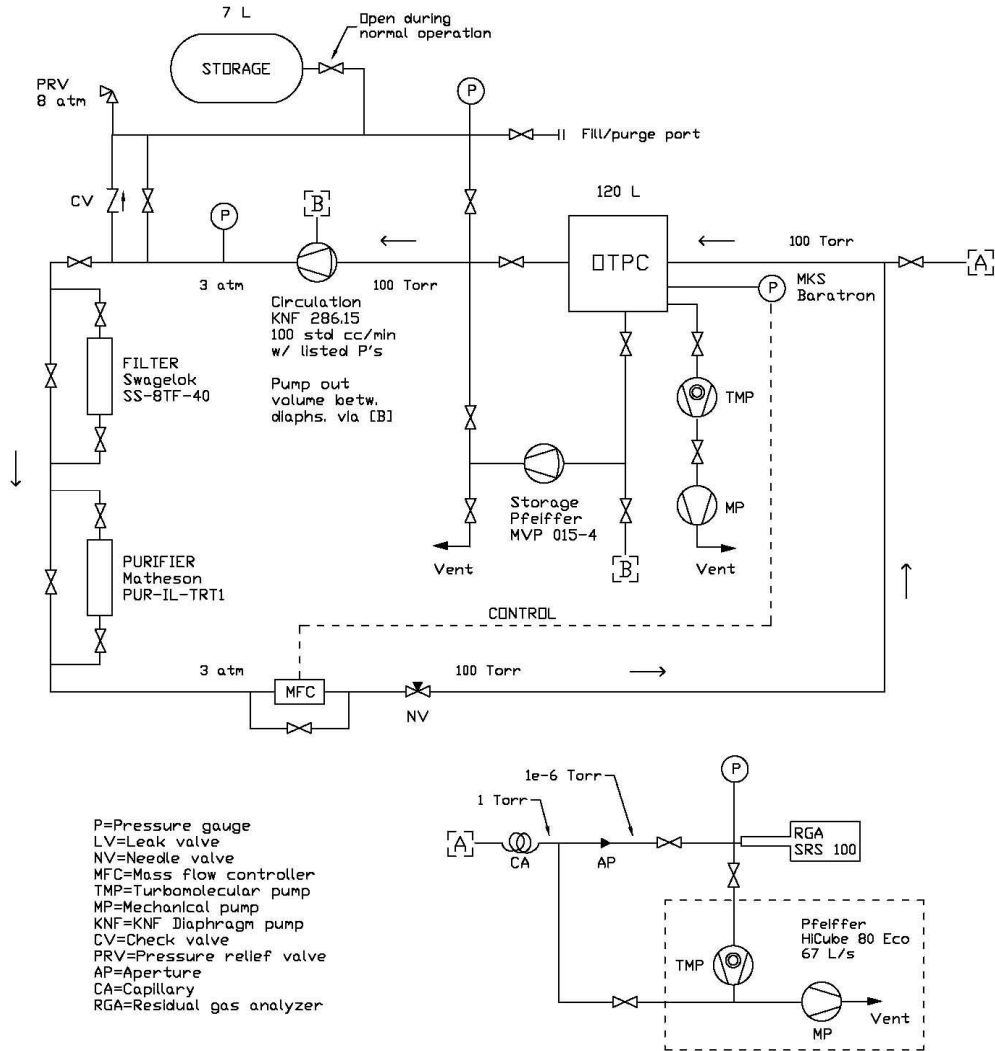


Fig. 11 - The gas handling system for use of isotopically enriched gasses in the e-TPC detector.

The e-TPC detector with gas handling system will be mounted on a moveable cart as shown in Fig. 12. In Fig. 13 we show a three dimensional view of the internal structure of the e-TPC.

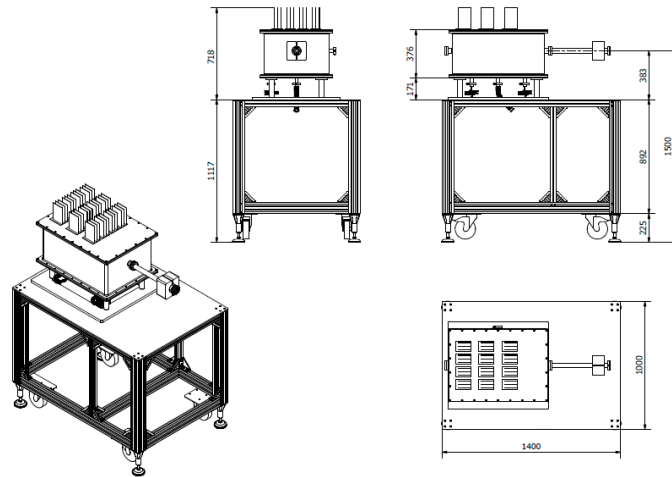


Fig. 12 - The movable cart for the proposed e-TPC detector.

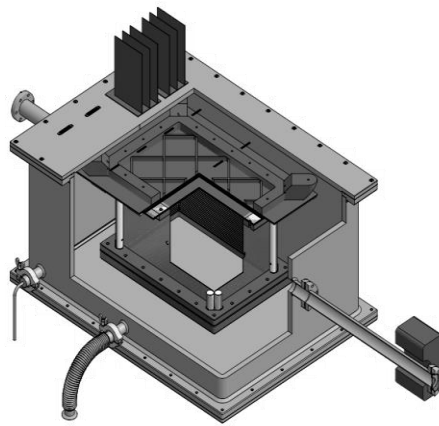


Fig. 13 – The internal structure of the proposed e-TPC detector.

The readout electronics of choice for the proposed e-TPC detector is the one developed by the Generic Electronics for Time Projection Chambers (GET) community [42]. In Fig. 14 we show the candidate electronic boards, which include

amplification and digitization that we propose to use for approximately 1000 channels of readout of the e-TPC. The details of the readout chain for a single channel are shown in Fig. 21.

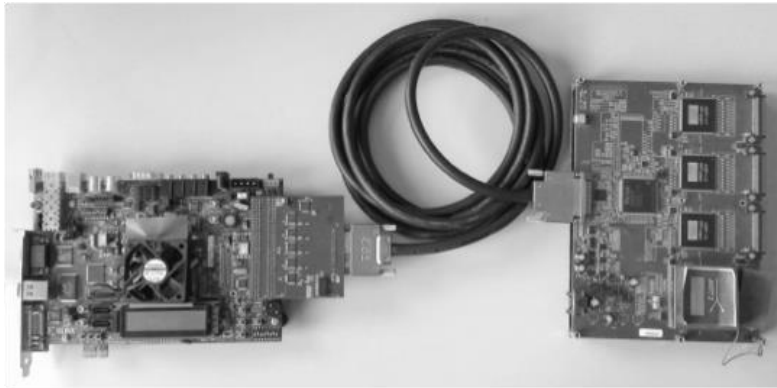


Fig. 14 - The proposed electronic readout of the e-TPC: a test bench for 256 channels consisting of one AsAd board and one Xilinx ML-507 board. Each AsAd board is equipped with 4 AGET chips (64 channels each) with integrated signal amplification, shaping, filtering and sampling stages. Source: *GET collaboration*.

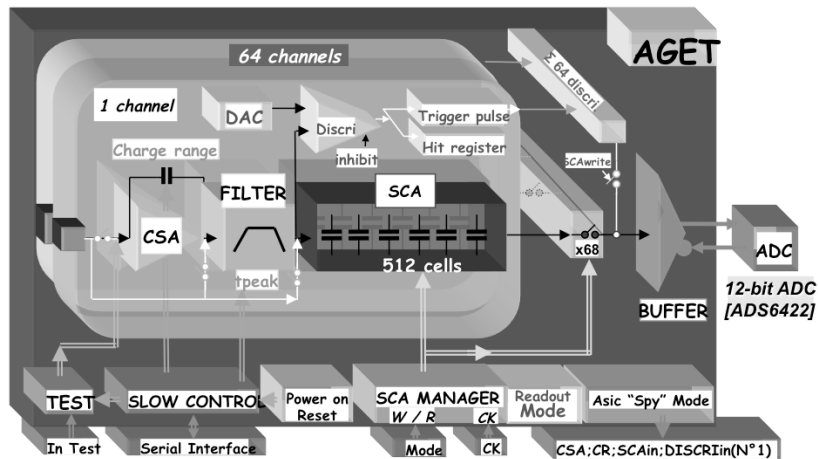


Fig. 15 - The proposed electronic readout of the e-TPC: a schematic of the readout chain of a single channel inside the AsAd board. After amplification and shaping the signal is sampled with user-selected frequency (between 1 MHz and 100 MHz) and stored in the Switched Capacitor Array (SCA) analog memory having 512 cells. Upon event acceptance signal, the SCA is frozen and a 12-bit ADC reads out SCA cells at the speed of 25 MHz. Source: *GET collaboration* [42].

The readout electronics for the active target gaseous e-TPC has to meet several criteria, as detailed below:

- adequate sampling frequency and number of sampling points per channel stored in a memory buffer;
- sufficient pulse-height resolution and signal dynamic range;
- uniform response across all the channels;
- signal shaping, filtering and amplification;
- external triggering (for measurements with beam) and self-triggering (for calibration runs with radioactive sources);
- reasonable cost per channel.

The limiting requirements for the electronics, such as the maximal sampling frequency at a fixed size of the memory buffer, are determined by the working conditions of the e-TPC detector (e.g. gas mixture composition, gas pressure and temperature, electric fields applied to drift and amplification regions). In addition, for projects of R&D nature like this one, additional constraints arise when the same type of electronics is going to be used for tests and for measurements with different gas mixtures under both atmospheric- and low pressure.

The UW group investigated the option of using the electronics already developed by the GET community. The international GET collaboration consist of permanent scientists, researchers and engineers from 3 French and 1 USA institutions: Centre Etudes Nucléaires de Bordeaux Gradignan (CENBG – Bordeaux, France), Grand Accélérateur National d'Ions Lourds (GANIL – Caen, France), Institut de Recherche sur les lois Fondamentales de l'Univers (IRFU – Paris, France) and National Superconducting Cyclotron Laboratory (NSCL/MSU – Lansing, MI, USA). The main goal of the GET project was to develop a new and complete electronic system with unprecedented capabilities for triggering, data read out and data event-rate processing. The first prototype components were tested in 2010 and the mass production of the final electronics modules has started in 2014. As of March 2015 there are over 20 experimental groups that use (or ordered) a GET system for their detectors. The possibility of exchanging information and experience on hardware and software among many users represents a clear and obvious advantage. Developers of the GET electronics will continue to provide technical support to laboratories that use GET electronics in the coming years.

The core component of the GET electronics is a custom-made 64-channel ASIC chip called AGET (*ASIC for GET*) that employs Switched Capacitor Array (SCA) fast analog memory. Four AGET chips are mounted on a single front-end AsAd card (*ASIC and ADC*). Its main features are the following:

- up to 256 channels in a single board;
- charge preamplifiers with 4 programmable gains per channel (120 fC – 10 pC);

- shaping amplifiers with 16 programmable time constants per channel (50 ns – 1  $\mu$ s);
- SCA analog, circular buffers with 512 cells (sampling points) per channel;
- adjustable sampling frequency of SCA buffers (1 – 100 MHz);
- 12-bit ADC with dynamic range of  $2 V_{p-p}$  and with fixed sampling frequency of 25 MHz for reading SCA memories (one ADC channel per AGET chip);
- possibility to bypass charge- and/or shaping amplifier;
- self and external triggering, hit counting and test pulse injecting capabilities.

The GET electronics system can be purchased in two variants: “full” or “reduced” set-up.

The more expensive “full” system is scalable up to 30720 channels and can process events at a maximum trigger rate of 1 kHz. It also requires between 1 and 3 micro-TCA chassis in order to operate.

The “reduced” GET system costs about 30 USD/channel. A single “reduced” system can serve up to 256 channels and consists of: 1 AsAd board with 4 AGET chips, VHDCI signal cable, reduced-CoBo to AsAd adapter card and Xilinx ML-507 board with PowerPC functionality. It is possible to extend the number of channels to 512 (or more) by synchronizing two (or more) ML-507 readout boards using common external trigger and clock signals. The lower cost per channel, with respect to entirely FPGA-based digitizing electronics, comes at the price of a lower number of sampling points due to SCA limitations. Still, the memory buffer of 512 cells provides decent spatial resolution of 0.4 mm even for the longest tracks that can fit in the drift region of 20 cm length that is foreseen in the e-TPC detector. Upon positive verification of the GET electronics characteristics with the mini-e-TPC detector, currently being built and tested under a separate one-year R&D contract between the UW group and ELI-NP, such electronics modules can be used in the full-scale e-TPC detector proposed in this TDR.

The complete detector system will include:

- data acquisition (DAQ) system able to handle all signals from the detector (at 100 Hz trigger rate envisaged for the  $\gamma$ -ray beam at ELI-NP) and all external monitors (e.g. beam energy, beam intensity);
- temperature and pressure monitor, which will be implemented into the DAQ system;
- detector for monitoring the drift velocity of electrons in the gas, which will be implemented into the DAQ system;

The e-TPC detector will be built and tested in Warsaw, where physicists and engineers have already the needed experience and the laboratories are equipped for the task. The gas system will be constructed by the UConn group at the ELI-NP facility in collaboration with ELI-NP personnel. The commissioning of the e-TPC will be done in ELI-NP.

### 2.2.1 Proof-of-principle studies and readiness

Since 2013, exploratory studies and laboratory tests using the model prototype detector equipped with electronics developed for plasma diagnostics in tokamaks and signal read-out with an oscilloscope produced encouraging results [43, 44]. These results set the ground for designing the research plan for this project. Among the results, a satisfactory energy resolution was achieved for the detection of X-rays from a  $^{55}\text{Fe}$  source using a read-out electrode with strips rotated by  $60^\circ$ . A measurement of alpha particles from natural radon accumulated on a filter, using multi-channel read-out electronics designed for the JET Tokamak facility (UK), allowed to verify the correlation between the coordinate perpendicular to the readout electrodes and drift velocity for the charge. Tracks of alpha particles were successfully reconstructed in 3D, see Fig. 16. The results of these proof-of-principle studies confirm the validity of the read-out method to be implemented in e-TPC detector for ELI-NP [34, 45, 46].

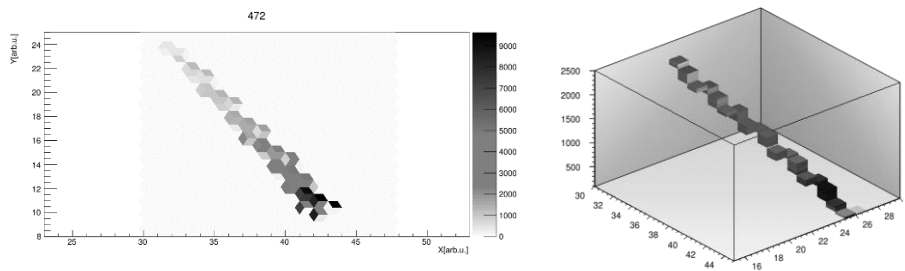


Fig. 16 - Examples of reconstructed alpha tracks with the model detector. Left panel: 2D-projection of track on the read-out plane integrated over time. Right panel: 3D reconstruction of a track. The gray scale corresponds to the measured energy deposits along the tracks.

Monte Carlo simulations of the detector response to the intense beam of  $\gamma$ -rays show that charged-particle events, e.g. the alpha particle emitted in the photo-dissociation of  $^{16}\text{O}$ , can be clearly separated from the beam-induced background and the difference is such that a selective trigger can be applied to accept only charged-particle events of interest. The energy deposited by  $10^7$   $\gamma$ -rays at 8 MeV in  $20 \times 20 \times 35 \text{ cm}^3$  gas volume filled with pure  $\text{CO}_2$  gas at 100 mbar was simulated with GEANT4.

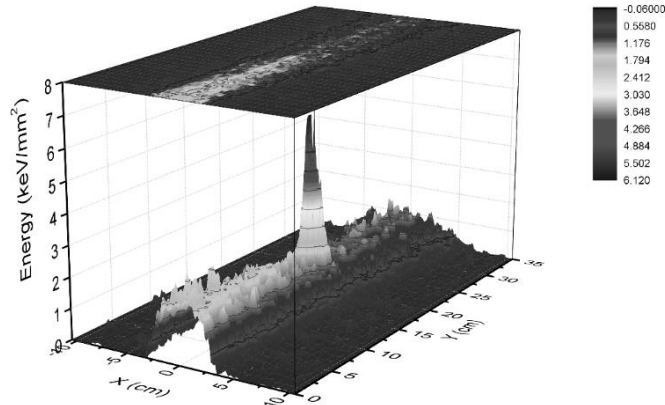


Fig. 17 - GEANT4 simulation of the  $\gamma$ -beam induced background (mainly electrons from gamma conversion in the entrance window) during a single macro-bunch in the e-TPC detector filled with  $\text{CO}_2$  gas at 100 mbar. A track of 0.5 MeV  $\alpha$  particle has been superimposed to mimic an interesting event of photo-dissociation of  $^{16}\text{O}$ . The gray scale corresponds to the integrated energy deposits on the 2D readout plane. The figure catches the most unfavorable case and the material, thickness, distance of the entrance window (and magnetic field provided by a permanent magnet) will be subject of optimizations.

Fig. 17 shows the dependence of this energy on the position on the readout plane (each bin corresponds to  $1 \times 1 \text{ mm}^2$  area). The structure visible in the middle of the readout plane represents the artificially superimposed signal from a single 0.5 MeV alpha particle emitted parallel to the readout plane at an angle of  $45^\circ$  with respect to the beam direction.

These pilot studies carried on at the University of Warsaw are continuing by means of the 1-year Research Project Contract signed between IFIN-HH/ELI-NP and the University of Warsaw within the framework of “Charged Particle Detection at ELI-NP” Working Group (ELI-NP Contract No. 3 of 01/10/2014).

Some Research & Development effort will be needed to integrate the existing GET electronics components with the e-TPC readout system. The scope of work includes among others: ensuring proper protection of the ASIC chips, minimizing parasitic capacitances and cross-talks in signals lines, allowing flexibility in trigger decision making, synchronizing pieces of data from several front-end AsAd cards in the event builder. Moreover, it can be beneficial to, both, the ELI-NP facility and the GET collaboration to join their efforts on replacing some legacy components of the “reduced” GET system for experiments that need only moderate number of channels (approximately 1000) and, therefore, do not want to invest in expensive infrastructure of the “full” GET system. In particular, the Xilinx ML-507 board (initially intended only as a test platform for developing larger, custom-made

FPGA-based board for the “full” version of the GET system) can be replaced with an up-to-date FPGA technology that will likely be still available on the market during next 2 – 3 years. The Warsaw group has already started discussing possible scopes of such R&D with the GET community and has received a positive feedback. Another aspect of employing the GET electronics is the synergy of knowledge and expertise between e-TPC and SSD experimental groups. For instance, the AsAd front-end cards are also suitable to read-out silicon detectors since they can handle, both, negative- and positive analogue input signals and offer great level of configurability in terms of: gain, filtering and sampling rate. Later this year the Catania group plans to perform dedicated proof-of-principle studies to confirm usefulness of the GET electronics for a solid target SSD array proposed in this TDR.

### 2.2.2 Staged implementation

The main goal of developing the e-TPC detector is to measure reaction cross sections for photo-dissociation reactions at the relevant astrophysical energies or close to (Section 2.2). The detector will be used also for nuclear structure studies (Section 2.1) and, by employing a tissue-equivalent gas mixture, for studies in nanodosimetry and radiation damage to DNA (see the Medical Applications TDR, ELI-NP RA4-TDR5). After completion of the main part of the scientific program, the detector can be reconfigured to run at higher pressures (a few bars). This thicker target will not allow to detect angular correlations between the reaction products, but it will allow to measure the total cross section for nuclear reactions in a *counting-experiment* mode, permitting to reach even lower interaction cross sections at energies below those needed for the full tracking operation mode running at 100 mbar. For example the very important measurement of the total ( $E_1 + E_2$ ) cross section of the  $^{12}\text{C}(\alpha, \gamma)$  reaction at lower energy with  $E_\gamma = 7.96$  MeV ( $E_{\text{cm}} = 0.8$  MeV) will be possible using three weeks of beam time with  $\text{CO}_2$  gas at 2 bars.

## 3. ESTIMATE OF COUNT RATES/FEASIBILITY OF PROPOSED DEVICES

### 3.1 The Silicon Strip Detector

#### *Count rates*

The SSD array is very suited for the measurement of all reactions induced by gamma rays on nuclear species that cannot be found in gas form. This is particularly important in the case of heavy ions that are synthesized in explosive environments

where photon induced reactions play an important role. For some key reaction like  $^{12}\text{C}$  photo-dissociation, the use of two complementary approaches (e.g., solid target plus SSD array and TPC detector) would be crucial to reduce systematic errors that contribute differently in the two analyses. One of the examples of a photo-dissociation process requiring a solid target to be investigated is the  $^{24}\text{Mg}(\gamma,\alpha)^{20}\text{Ne}$  reaction.

Assuming a conservative beam intensity of  $5 \times 10^3$   $\gamma/\text{s/eV}$ , beam width of 0.5%, target thickness  $2.5 \times 10^{18}$  atoms/cm<sup>2</sup> (corresponding to a 100  $\mu\text{g}/\text{cm}^2$  – thick  $^{24}\text{Mg}$  target), we expect a count rate of 0.35 counts/s at the gamma energies of interest (around 11.6 MeV), corresponding to about  $3 \times 10^4$  reaction events per day. These numbers make it clear the presence of a significant signal and the possibility to measure the cross section of the  $^{24}\text{Mg}(\gamma,\alpha)^{20}\text{Ne}$  reaction even in the realistic case that such cross section is 10 times lower than the predictions based on the statistical approach.

### ***Beam quality requirements from ELI-NP and the feasibility of astrophysics experiments***

However, in this kind of measurements the relevant parameter ensuring the feasibility of the experiment is the signal-to-noise ratio. Therefore, careful simulations of beam-induced background play a key role especially because low detection thresholds are needed to fully reconstruct the reaction kinematics. Using a solid  $^{24}\text{Mg}$  target, 100  $\mu\text{g}/\text{cm}^2$  thick to reduce energy straggling of the outgoing alphas, deposited onto a 60  $\mu\text{g}/\text{cm}^2$  thick carbon backing, a major source of background would be electrons, positrons and gamma rays from Compton and photoelectric effects and pair production. Of course, at approx. 11 MeV the photoelectric contribution on  $^{24}\text{Mg}$  is negligible.

Fig. 18 shows the angular distributions of photons emitted following the gamma beam interaction with the target plus backing system, including all the photon production mechanisms. This spectrum was obtained by implementing the beam and target features into a GEANT4 simulation code and selecting the energy where the photon distribution has a sharp maximum. It was obtained for  $6 \times 10^8$  impinging photons, approximately equal to the amount of gammas hitting the target in 2 seconds. Clearly, the background event rate is rather small. Moreover, in a 150 micron silicon detector only 0.2% of these photons would interact at 1 MeV (where the energy distribution has a maximum) inducing a very small signal since the Compton effect is dominant. We predict an energy deposit as small as few keV. We can conclude that photon background on silicon detectors would be negligible, introducing a negligible threshold on detectors.

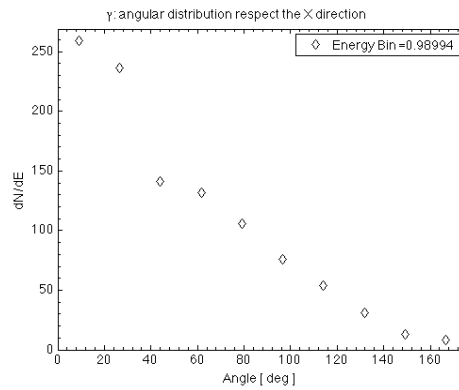


Fig. 18 - Angular distribution of photons emitted following the gamma beam interaction with the target plus backing system.

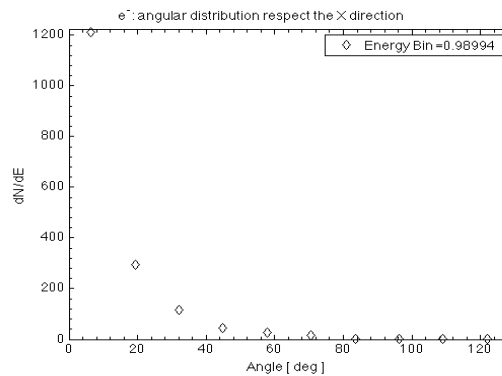


Fig. 19 - Angular distribution of electrons emitted following the gamma beam interaction with the target plus backing system.

Similarly, Fig. 19 shows the angular distribution of electrons emitted following the gamma beam interaction with the target plus backing system, including all the electron production mechanisms. We expect about 600 electrons/s at small angles, about 10 degrees, with energies of few MeV. At these energies electrons are already minimum ionizing particles in silicon, with stopping powers smaller than 0.5 keV/ $\mu\text{m}$ . The signal induced by such electrons on 150 micron silicon detectors is smaller than 80 keV, making electron induced background and detection threshold negligible. The same discussion applies to positrons.

It is important noting that particle identification and background suppression, due to reactions on impurities and especially on the target backing, can be effectively achieved if the reaction kinematics is recorded, since the  $^{24}\text{Mg}(\gamma,\alpha)^{20}\text{Ne}$  reaction is a binary process. This is possible because at a known fixed angle alphas are emitted with a well-determined energy, making it possible to gate on this region to determine the differential cross section. For instance,  $^{12}\text{C}$  photo-dissociation leads to  $3\alpha$ 's in the exit channel ( $Q = 7.27$  MeV), with a reaction kinematics totally different from the one of a two-body process. Simulations show that  $3\alpha$  kinematics is smooth, thus easily separable from the  $^{24}\text{Mg}(\gamma,\alpha)^{20}\text{Ne}$  one. The same discussion applies for photon.

### 3.2 The e-TPC Detector

The experimental rates and relative beam time needs were estimated for the four astrophysical – relevant reactions considered as priority in the e-TPC scientific program and described in Section 2.2. An average beam intensity of  $2.5 \times 10^4$   $\gamma$ /s/eV, beam width of 0.5% and 100 mbar gas density were considered in each case. The beam intensity is the mean value of the spectral density  $0.8 - 4 \times 10^4$   $\gamma$ /s/eV given in the Gamma Beam System specifications [47].

Table 1  
Beam time requirements for the e-TPC measurements

Reaction	$E_\gamma$ [MeV]	$E_{c.m.}$ [keV]	Gas mixture	Rate [events/day]	Beam- time estimate	Goal
$^{16}\text{O}(\gamma,\alpha)^{12}\text{C}$	8.26	1.1	$\text{CO}_2$	70	21 days	Determine angular distribution
$^{19}\text{F}(\gamma,p)^{18}\text{O}$	8.08	90	$\text{CF}_4$	5	14 days	Determine the resonance strength
$^{22}\text{Ne}(\gamma,\alpha)^{18}\text{O}$	10.137 10.233	470 566	$^{22}\text{Ne}$	24 170	14 days 7 days	Determine the resonance strengths
$^{21}\text{Ne}(\gamma,\alpha)^{17}\text{O}$	8.01 8.06 8.47 8.66	661 715 1123 1312	$^{21}\text{Ne}$	few events/day <sup>1</sup> few tens events/hour	14 days 14 days 1 day 1 day	Determine the resonance strengths (8.01 and 8.06 MeV) and spin and parity (8.47 and 8.65 MeV)

<sup>1</sup> assuming that the resonance strength is larger than 1  $\mu\text{eV}$ .

## 4. SPECIFIC NEEDS AND UTILITIES, TRANSVERSAL NEEDS

### 4.1 The SSD

#### *Infrastructure:*

- Electronic and mechanical workshops;
- Clean area for detector storage and assembly;
- Radioactive sources for detector testing and calibration.

### 4.2 The e-TPC Detector

#### *Infrastructure:*

- Electronic and mechanical workshops;
- High speed, 10Gb/s Ethernet or Infiniband data connection from experiment to control/data acquisition room; interface with the experiment to be developed;
- High speed data storage system;
- Radioactive sources for detector testing and calibration;
- Clean area for detector storage and assembly;
- Remotely controlled e-TPC support at E8 area.

### 4.3 Generic ELI-NP Infrastructure

#### *Gamma Beam Characteristics*

The detectors design and the rate estimates presented in this document were performed assuming the gamma beam parameters foreseen. As mentioned in the technical description of the e-TPC detector, the possibility to rotate the linear polarization plane and eventually the possibility to use circular polarization of the gamma beam would be beneficial for the accuracy of the measurements.

#### *Control Systems*

The ELI-NP E8 area will be partially dedicated to Charged particles experiments using the SSDs detectors array and the e-TPC detector. This area will have the experiment monitoring and control systems architecture similar to the GBS and GBDD control systems. The architecture is based on EPICS which will permit local distributed control of the equipment and additional clients to remotely supervise/control the experiment.

This solution will allow a standardization of the control systems inside ELI-NP, while providing easy maintenance, better security, better logging and interfacing methods between the experimental areas, GBS and GBDD.

A dedicated User-Room will be used to remotely control from outside the E8 area the equipment as the experiment is running. An EPICS framework will be developed to link the experimental area to the User-Room using a dedicated client-server architecture that will allow maintenance and upgrades to be performed without interacting with other systems.

A data storage server will be available for short term experimental data saving and this shall benefit in general from dedicated data busses, separated from the client-server EPICS architecture that controls and monitors the equipment itself, in order to achieve the highest data throughput.

Dedicated EPICS servers are envisaged to interface the equipment necessary in the experiment such as:

- Bias Voltage system for the SSDs detector array;
- High Voltage system for the eTPC detector;
- Temperature and pressure monitoring system for the eTPC detector;
- Drift-velocity monitoring system for the eTPC detector;
- Gas recycling system including vacuum for the eTPC detector;
- DAQ system for the SSDs detector array;
- DAQ system for the e-TPC detector.

Each of the above equipment will have a Human Machine Interface able to locally (from inside the interaction area) or remotely (from the User-Room) monitor and control the parameters needed to run the equipment and the experiment.

For the equipment where the API is not provided, or the required development time does not fit into the general schedule, the link between the User-Room and the experimental area will be made using remote desktop (or similar) and by using their proprietary software.

The User-Room will also provide through the EPICS architecture information to the user regarding the GBS parameters and GBDD configuration. The GBS and GBDD parameters will be controlled from the Gamma control room by the operators from personnel and machine safety reasons.

### ***Data acquisition, processing and storage***

As detailed in the ELI-NP Monitoring and Control Systems TDR, the data flow architecture at ELI-NP is split in two parts, one on the Experiment side and one on the facility infrastructure side (see Fig. 20 below).

### *Utilities*

According to the general lines followed in the ELI-NP buildings design, the maximum versatility of the electrical power, liquid nitrogen and compressed air supplies could only be achieved by letting the last (user-end) part of these networks to be built by each experimental area. That is, in the case of each utility type:

- Electrical power: a connection point of a certain maximum power rating, three-phased, is defined at the exterior of each experimental room. At this point, a distribution panel must be fitted, constructed according to the requirements of the experiments TDRs. Then, according to the same, the distribution inside the experimental areas must be designed and built. For the E8 experimental area, where the detectors proposed in this TDR are to be used, the maximum power rating is 50 KW;
- Liquid nitrogen: a connection point will be available beneath each experimental hall, in the basement (under the stabilization concrete plate);
- Compressed air: connection points will be defined in the basement of the building, being the experiments' responsibility the distribution network for each experiment.

Cooling water: two heat exchangers for closed-circuit water cooling will be available in two locations, in the basement of the building, under the laser system and the electron accelerator areas. The connection to these and the following network to the, and inside, the experimental hall is in the responsibility of the TDR workgroups.

The characteristics of electrical power of high stability are still subject of discussions between the TDR workgroups and the ELI-NP engineering and building teams. There will be available in the ELI-NP experimental building two separate networks, one for heavy duty and the second devoted to sensitive detection systems and electronics. The two networks will have as an electrical ground a mesh of copper bars connected to the steel bars in the stabilized concrete plate (which are soldered together), that is then linked to the earth connections foreseen around the building. This "mesh-type" approach will provide a solid base for the achievement of a reliable ground connection.

The infrastructure will feature an electrical generator that shall be started in case of blackout, while each experiment shall foresee adequate UPS capacity to hold until the operation in full of the generator and/or until safe shutdown of all equipment.

The detectors shall be placed in the E8 experimental hall (see Fig. 21). Each of them will be designed according to the ELI-NP specifications regarding mobility,

in order to accommodate on the positioning mechanisms in E8 and be able to be positioned out of the beam to a storing place when not in use.

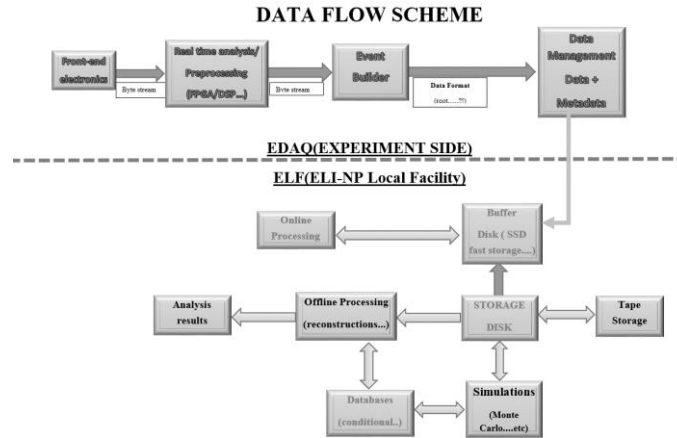


Fig. 20 - Data flow scheme  
(from the ELI-NP Monitoring and Control Systems TDR).

### *Floor space requirements and positioning*

The experimental setups will also have the possibility to be positioned in a row along the gamma beam direction, due to their relative transparency to this radiation. The total floor space occupied by the two detectors is approximately 10 m<sup>2</sup>, including the auxiliary equipment (vacuum, part of the electronics).

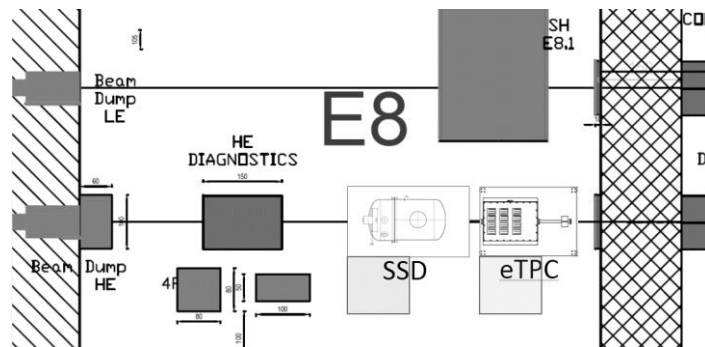


Fig. 21 - Schematics of the E8 experimental area  
(with the SSD and e-TPC in beam).

***Background and shielding***

At this point, no special shielding of the detectors is foreseen for the operation in the beam. The background radiation generated by the gamma beam dump also located in E8 shall be very low, as preliminary simulations show.

During setup of the experiments, the use of radioactive calibration sources may prompt in some cases for the use of local shielding depending on the type and activity of such sources.

***Other infrastructure – related needs:***

- Collimators and shielding materials;
- Electrical power of high stability;
- Mechanics of the detector support in the beam-line – movable table allowing a remote control of the detector positioning in the beam axis;
- Cable ducts;
- Disk storage;
- Fast internet transmission lines;
- Central CPU for off-line data processing;
- Beam-energy profile and beam-intensity information to be integrated into the DAQ.

## 5. SAFETY REQUIREMENTS

Standard electrical (high voltage) and mechanical safety rules shall be obeyed at all times when working on, or operating, the detectors.

### 5.1 The Silicon Strip Detector

For the calibration of the SSD array  $^{214}\text{Am} - ^{242}\text{Cm}$  sources will be employed, with low activities of the order of nCi.

### 5.2 The e-TPC Detector

Pressurized gas containers will be used at ELI-NP for the refilling and maintaining the pressure in the drift chamber of the e-TPC, possibly flammable gases to be employed.

During the commissioning of the e-TPC and for calibration purposes, very weak alpha radiation sources will be used, with activities below 1 kBq. Collimated, they will provide counting rates of some tens of Hertz, adequate for calibration procedures. Proposed sources are  $^{241}\text{Am}$ ,  $^{228}\text{Th}$  and  $^{148}\text{Gd}$ .

## 6. COLLABORATIONS

The development of the SSD array for ELI-NP is performed by a collaboration between ELI-NP and INFN-LNS (Istituto Nazionale di Fisica Nucleare – Laboratori Nazionali del Sud). Preliminary development of the setup and testing of the Micron SSD's and related electronics chain has begun at the National Institute of Physics and Nuclear Engineering in Romania (IFIN-HH) and INFN-LNS. Tests will be performed at IFIN's Tandem accelerator and other facilities. An R&D contract was signed between IFIN-HH/ELI-NP and INFN-LNS for the design of the detector and testing of the electronics.

The e-TPC design is performed by an international collaboration of the University of Warsaw with the University of Connecticut and ELI-NP. MoUs were signed between these institutions. The design, construction, test and delivery to ELI-NP of a mini-e-TPC with 128 channel readout (and extension to 256 channels) is in progress in the framework of a Research & Development contract between the ELI-NP and the University of Warsaw was signed.

*Acknowledgements.* O.T., C.B., S.G., D.G.G., C.M., and C.P. were supported by the Project Extreme Light Infrastructure - Nuclear Physics (ELI-NP) - Phase I, a project co-financed by the Romanian Government and European Union through the European Regional Development Fund. M.G. and D.P.K. acknowledge support from USDOE award No. DE-FG02-94ER40870.

## REFERENCES

1. D. Filipescu *et al.*, Eur. Phys. J. A, in press.
2. M. Kamimura, Nucl. Phys. A **351**, 456 (1981).
3. Y. Funaki *et al.*, Phys. Rev. C **80**, 064326 (2009).
4. R. Roth *et al.*, Phys. Rev. Lett. **107**, 072501 (2011).
5. A. C. Dreyfuss *et al.*, Phys. Lett. B **727**, 511 (2013).
6. E. Epelbaum *et al.*, Phys. Rev. Lett. **106**, 192501 (2011).
7. E. Epelbaum *et al.*, Phys. Rev. Lett. **109**, 252501 (2012).
8. M. Chernykh, H. Feldmeier, T. Neff, P. von Neumann-Cosel, and A. Richter, Phys. Rev. Lett. **98**, 032501 (2007).
9. Y. Kanada-Enyo, Prog. of Theo. Phys. **117**, 655 (2007).
10. H. Morinaga, Phys. Rev. **101**, 254 (1956).
11. M. Itoh *et al.*, Nucl. Phys. A **738**, 268 (2004); Phys. Rev. C **84**, 054308 (2011).
12. M. Freer *et al.*, Phys. Rev. C **80**, 041303(R) (2009).
13. W.R. Zimmerman *et al.*, Phys. Rev. C **84**, 027304 (2011).
14. M. Freer *et al.*, Phys. Rev. C **86**, 034320 (2012).
15. H.O.U. Fynbo and M. Freer, Physics **4**, 94 (2011).
16. W.R. Zimmerman *et al.*, Phys. Rev. Lett. **110**, 152502 (2013).
17. M. Gai *et al.*, JINST **5**, 12004 (2010).
18. M. Freer *et al.*, Phys. Rev. C **76**, 034320 (2007).

19. M. Freer *et al.*, Phys. Rev. C **83**, 034314 (2011).
20. O.S. Kirsebom *et al.*, Phys. Rev. C **81**, 064313 (2010).
21. W.A. Fowler, Rev. Mod. Phys. **56**, 149 (1984).
22. S. Dababneh *et al.*, Phys. Rev. C **68**, 025801 (2003).
23. C. Iliadis, Nuclear Physics of Stars (Weinheim: Wiley-VCH Verlag, 2007).
24. H. Lorenz-Wirzba *et al.*, Nucl. Phys. A **313**, 46 (1978).
25. M. Wiescher *et al.*, Nucl. Phys. A **349** 165 (1980).
26. C. Angulo *et al.*, Nucl. Phys. A **656**, 3 (1999).
27. M.Q. Buckner *et al.*, Phys. Rev. C **86**, 065804 (2012).
28. A. Best *et al.*, Phys. Rev. C **83** (2011) 052802(R).
29. S.D. Pain *et al.*, AIP Conf. Proc. **1090**, 570 (2008).
30. M. Matos *et al.*, PoS (NIC XI), p. 226., 2011
31. Micron Semiconductor – general catalogue, <http://www.micronsemiconductor.co.uk/pdf/cat.pdf>.
32. J.A. Duenas *et al.*, Nucl. Instr. Meth. A **676**, 70 (2012).
33. K. Miernik *et al.*, Nucl. Instrum. Methods A **581**, 194 (2007).
34. J. Bihałowicz *et al.*, *3D reconstruction of nuclear reaction using GEM TPC with planar readout*, Proc. of the Carpathian Summer School of Physics 2014, Sinaia, Romania, AIP Conf. Proc. **1645**, 301 (2015).
35. M. Ćwiok *et al.*, IEEE Trans. Nucl. Sci. **52**, 1895 (2005).
36. K. Miernik *et al.*, Eur. Phys. J. A **42**, 431 (2009) 431.
37. M. Pomorski *et al.*, Phys. Rev. C **83**, 014306 (2011).
38. M. Pomorski *et al.*, Phys. Rev. C **83**, 061303(R) (2011).
39. J. Rzadkiewicz *et al.*, 23-rd IAEA Fusion Energy Conference, Daejon, Republic of Korea, 2010.
40. J. Rzadkiewicz *et al.*, Proc. 2nd Intern. Conf. Front. in Diagnostic Technologies, Frascati, Italy, November 28-30, 2011, EFDA-JET-CP (11) 07/02.
41. J. F. Ziegler, M. Ziegler and J. Biersack, Nucl. Instr. and Meth. B **268**, 1818 (2010) <http://www.srim.org>.
42. E. Pollacco *et al.*, Physics Procedia **37**, 1799 (2012).
43. J. Rzadkiewicz *et al.*, Nucl. Instr. Methods A **720**, 36 (2013).
44. G. Kasproicz, Proc. of SPIE **8454**, 84540M (2012).
45. J. Bihałowicz, *The Conceptual Study of a Time Projection Chamber for Nuclear Reactions in Astrophysics*, B.Sc. thesis, University of Warsaw, 2014.
46. J. Bihałowicz *et al.*, *3D imaging of nuclear reactions using GEM TPC*, XXXIV-th IEEE-SPIE Joint Symposium, Wilga, Poland, 2014, Proc. of SPIE **9290**, 92902C (2014).
47. A. Variola, presentation at the ELI-NP Science Program and Instruments: *Technical Design*.